Lung lobe segmentation by anatomy-guided 3D watershed transform

Jan-Martin Kuhnigk*, Horst K. Hahn, Milo Hindennach,
Volker Dicken, Stefan Krass, and Heinz-Otto Peitgen

MeVis — Center for Medical Diagnostic Systems and Visualization
Universitaetsallee 29, 28359 Bremen, Germany

ABSTRACT

Since the lobes are mostly independent anatomic compartments of the lungs, they play a major role in diagnosis and therapy of lung diseases. The exact localization of the lobe-separating fissures in CT images often represents a non-trivial task even for experts. Therefore, a lung lobe segmentation method suitable to work robustly under clinical conditions must take advantage of additional anatomic information. Due to the absence of larger blood vessels in the vicinity of the fissures, a distance transform performed on a previously generated vessel mask allows a reliable estimation of the boundaries even in cases where the fissures themselves are invisible. To make use of image regions with visible fissures, we linearly combine the original data with the distance map. The segmentation itself is performed on the combined image using an interactive 3D watershed algorithm which allows an iterative refinement of the results. The proposed method was successfully applied to CT scans of 24 patients. Preliminary intra- and inter-observer studies conducted for one of the datasets showed a volumetric variability of well below 1%. The achieved structural decomposition of the lungs not only assists in subsequent image processing steps but also allows a more accurate prediction of lobe-specific functional parameters.

Keywords: pulmonary imaging, lung lobes, lobar fissures, segmentation, watershed transform, CT imaging

1. INTRODUCTION

The human lungs are composed of distinct anatomic compartments called *lobes*. Since they represent functional units, the lobes have their own bronchial and vascular systems. These systems are solely connected close to the *hilus*, which is defined as the area where bronchi as well as the pulmonary arteries and veins enter the lungs. The lobes in each lung are separated by thin tissue, the so-called *lobar fissures*. As shown in Figure 1, an *oblique fissure* and a *horizontal fissure* divide the right lung into *upper*, *lower*, and *middle lobe*. In the left lung there is only an oblique fissure separating lower and upper lobe.

A robust and reproducible lobe segmentation would not only provide boundaries for further segmentation steps and yield landmarks for registration procedures, but would also allow a lobe-based CT parameter extraction and thus a more accurate prediction of post-operative lung function in case of a lobar resection, which is the standard treatment for early stage lung cancer. However, there is little or no lobar quantitation support available in existing pulmonary image processing software. First of all, a manual segmentation of the fissures in CT volume data is not feasible due to the large number of slices in a typical CT scan. Second, computer-aided methods have to deal with the fissures' low contrast and variable appearance, which, in some cases, makes it impossible to determine their exact location even for experts. Measuring about one millimeter in thickness, the lobar fissures only show up as thin bright lines on high resolution CT images (Fig. 2 a–c). For lower resolution scans which are still widely used due to old scanning devices or for dose reduction, the fissure density averages with the surrounding parenchyma and the fissures merely appear as diffuse clouds of slightly higher density in an area with little or no vasculature (Fig. 2 d). Furthermore, as described by Hayashi et al.,[1] various pulmonary diseases can affect their imaging appearance. A single detection algorithm will have great difficulties to work robustly under clinical conditions, where a considerable amount of cases will show progressive widening, incompleteness

*Email: kuhnigk@mevis.de, URL: www.mevis.de.

The research leading to this publication has been supported by the German Federal Ministry of Education and Research under the grant number 01EZ0010. The authors take full responsibility for the content of this publication.

Medical Imaging 2003: Image Processing, Milan Sonka, J. Michael Fitzpatrick, Editors,
Proceedings of SPIE Vol. 5032 (2003) © 2003 SPIE · 1605-7422/03/$15.00

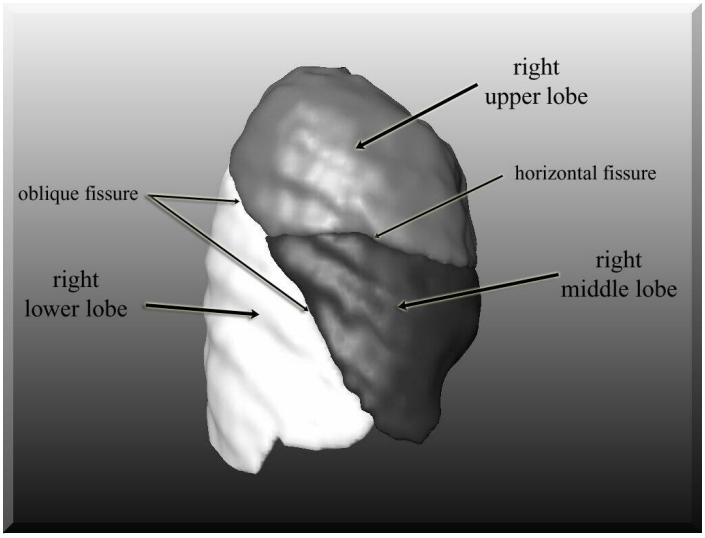

Figure 1. 3D surface rendering of the segmented lobes and the separating fissures in a sagittal view from the right at a normal right lung.

or even the absence of a fissure. Nearby tumors, atelectasis, or emphysematous changes can present additional problems for fissure segmentation algorithms.

Despite the difficulties, lobar segmentation techniques that rely mostly on fissure detection dominate the current literature in this area. An interactive method to extract the oblique fissures using a fuzzy reasoning system followed by a graph search has been developed by Zhang et al.[2] and later extended to include 3D shape constraints.[3] In contrast to resolving unclear situations by referring to morphological knowledge, the approach presented here overcomes these problems by using the structural knowledge of the lung anatomy, i. e. the quasi-autonomy of each lobe with respect to the vascular system.

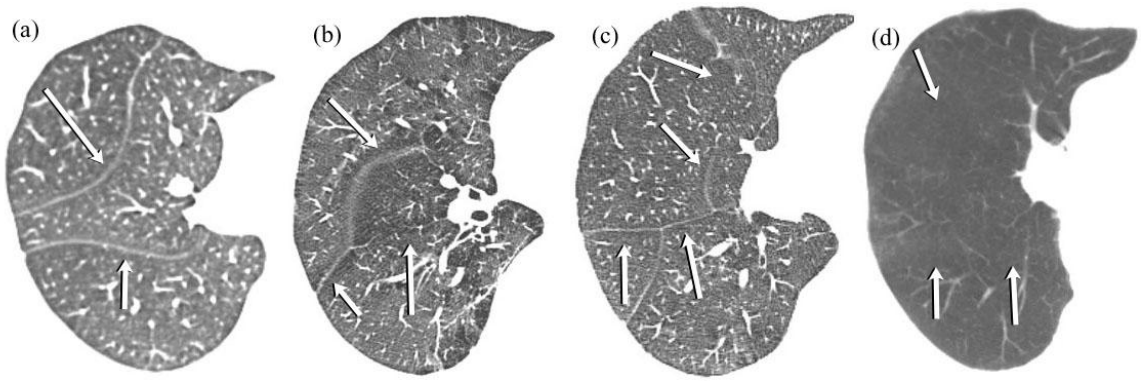

Figure 2. Four sample slices of right lungs of four different patients: (a) high resolution scan (slice thickness: 1.25 mm) showing almost perfectly traceable fissures; (b) high resolution scan (1.25 mm) of an emphysematous lung with partially disintegrating fissures; (c) high resolution scan (1.25 mm) of a lung with partially disintegrating fissures as well as an extra fissure branching off the oblique fissure; (d) low resolution scan (5 mm) of a lung with virtually no fissure contrast. Approximate fissure locations are indicated by the white arrows. Those directed upwards point at the estimated location of the oblique fissure, while the position of the horizontal fissure is indicated by arrows pointing right- and downwards.

After an automated lung segmentation procedure, a fast region growing algorithm is used to obtain a coarse vessel segmentation. The results are used to compute the Euclidean distance to the vascular system for each

voxel of the lung mask, locally emphasizing areas which show an absence of larger vessels. Being dependent on the vessels only so far, we introduce explicit fissure information contained in the original data (at least in high resolution images) by combining the original image linearly with the one obtained by the distance transform. Based on the resulting image, the lung lobes are segmented in the only processing step requiring user intervention: The Interactive Watershed Transform (*IWT*, Hahn *et al.*[4]). In this concluding procedure, markers can be used not only to identify the different lobes but also to interactively refine the results.

2. METHODS

We assume an input volume of integer dimensions $X \times Y \times Z$. The set of all voxel positions within the input volume is defined as $V := \{0, ..., X-1\} \times \{0, ..., Y-1\} \times \{0, ..., Z-1\}$, whilst $I := (i_v)_{v \in V}$ refers to the 3D input matrix. An entry i_v denotes the integer density value of the voxel v within the input volume. Possible values range from 0 to 4095 corresponding to Hounsfield Units (HU) between -1024 HU and 3071 HU. In case the world coordinates of a voxel v are used, we indicate this by writing world(v).

2.1. Lung Segmentation

Our lobe segmentation algorithm assumes the presence of a segmentation mask for each lung. Our lung segmentation procedure is fully automated and therefore does not add to the user input necessary for the lobar segmentation. However, since other methods exist[5] to fulfill this task and we would rather focus on the lobe segmentation, we only give a brief description of our lung segmentation algorithm.

1. **Segmentation of the airways**

   In order to prevent the region growing algorithm used for the parenchyma segmentation from running from one lung into the other through the low-density bronchial tree, the airways have to be segmented. We currently use the region growing variant proposed by Selle,[6] which is able to automatically determine a suitable upper threshold from the differential increase of the segmented volume. An algorithm specialized for the bronchial tree is currently under development.

2. **Lung separation**

   Unfortunately, the thoracic airways are not the only obstacle for a separation of the lungs. Predominantly emphysematous lungs tend to be inflated by the excessive lung pressure originating in the disease. Therefore, the left and the right lung are often in immediate contact, showing only a very thin border whose density, lowered by partial volume effects, falls below the upper threshold of -400 HU usually chosen for lung parenchyma segmentation. To allow a separation of the lungs even in those cases, a three-dimensional marker based watershed transform is used. The resulting masks can be used to block the respective regions in the following region growing step.

3. **Parenchyma segmentation**

   A fast and memory efficient implementation of a conventional 3D region growing algorithm is performed to obtain the parenchyma masks. Using the results generated in step 1 and 2, a global threshold interval of $[-1024, -400]$ HU and one automatically generated seed point per lung proved sufficient to obtain separate lung masks.

4. **Closing the lung masks**

   For most applications in pulmonary image processing, lung masks are needed that cover the vasculature being only partially segmented by the proposed parenchyma segmentation. Therefore, several kernel-based filters including morphologic closing were combined to close the gaps in the parenchyma masks.

5. **Extraction of volumes of interest**

   A *volume of interest (VOI)* is generated from the bounding box of each lung in order to reduce the amount of data that needs to be kept in memory at a time during subsequent image processing steps. When mentioning the input volume I or the associated set of voxels V in the following, we refer to the original chest dataset reduced to the VOI of the lung currently being processed.

2.2. Vascular Segmentation

The guiding principle in our method is to avoid a strict dependence on the fissure visibility in the patient's lung. As can be seen in figure 3, the absence of larger vessels in the areas indicated by the arrows already allows a visual estimate on the fissure locations without displaying the fissures themselves. To quantify this observation for computational use, a segmentation of the vasculature is needed.

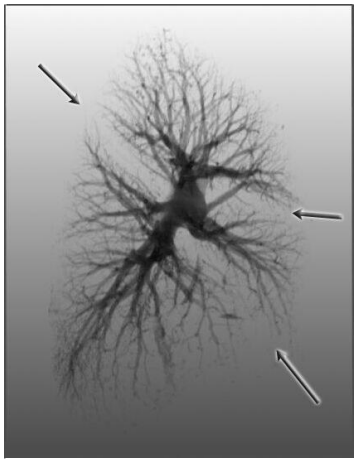

Figure 3. Sagittal 3D volume rendering of the segmented blood vessels of a right lung. The rareness of vessels in the areas indicated by the arrows allows an estimate of the fissure locations (see also figure 1).

The segmentation of the blood vessels can be restricted to the area defined by the lung mask. Because of the high contrast between the blood vessels and the parenchyma, a conventional 3D region growing algorithm is sufficient to obtain at least a superset of all larger pulmonary blood vessels. By searching the data for a bright area in the image region where the hilus is expected, a suitable seed point is automatically detected. A 6-neighborhood relation is used in combination with a fixed threshold to distinguish the vessels roughly from the parenchyma. The threshold should be adapted once for each specific scan protocol in order to avoid an over-segmentation which could include the fissures. Using this basic segmentation method, we evidently put up with the consequence that tumors and other bright unwanted structures, when connected to the vasculature, might be included in the resulting mask. We describe the resulting mask by a function $\mathrm{ves} : V \mapsto \{0, 1\}$ that maps each voxel v in V:

$$\mathrm{ves}(v) \;:=\; \begin{cases} 1, & \text{if } v \text{ was identified as a vessel voxel,} \\ 0, & \text{otherwise.} \end{cases}$$

2.3. Euclidean Distance Transform

To quantify the rareness of larger vessels in the lobar boundary areas, an Euclidean distance transform is performed. In other words, to compute the distance map $D := (d_v)_{v \in V}$, the Euclidean distance d_v of each voxel v in V to the closest vessel voxel is calculated. Note that each voxel's world coordinates were used in order to account for voxel anisotropy:

$$d_v \;:=\; \min \{ \| \,\mathrm{world}(v) - \mathrm{world}(v') \,\|_2 : \; v' \in V \;\wedge\; \mathrm{ves}(v') = 1 \} \,. \tag{1}$$

An example of a distance map is shown in the left part of Figure 4. To actually compute the distances, the multi-dimensional distance transform algorithm for digitized images proposed by Saito et al.[7] was used.

2.4. Refinement of the Distance Image

Although there are still plenty of older CT scanners in clinical use producing low resolution data, where the lobar fissures are more or less invisible, an increasing number of radiological facilities is equipped with multi-slice CT

scanners yielding high resolution images. In these scans, the fissures show at least partially a noticeably higher density than the surrounding parenchyma (Fig. 2 a, b, and c). Thus, we chose to refine the blurred structures visible in the distance image D (Fig. 4, left) with the sharp fissure contours possibly present in the original data (Fig. 4, right). This was achieved by performing a linear combination of D with the original I to a third volume $C := (c_v)_{v \in V}$:

$$C \ := \ I + \alpha * D, \qquad (\alpha > 0) \tag{2}$$

The general idea is for the (locally) relatively bright fissure voxels to fall together with already (locally) bright (that is, less close to the next segmented vessel than the surrounding voxels) areas in the distance image. For the linear combination of D and I resulting in the new volume C, two different values for the weighting parameters α have been experimentally adapted to the requirements of high and low resolution CT scans. Figure 4 shows the same slice on the three involved images to demonstrate the effect of the combination. In the distance image to the left, the fissure locations can be visually estimated but appear blurred, whereas in the original image to the right, the fissures can be traced in more detail but partially show little or no contrast. In the combined image however, the thin fissure lines are broadend and, where not visible, roughly continued by the influence of the distance image. This results in a more robust lobar separation in the following watershed transformation.

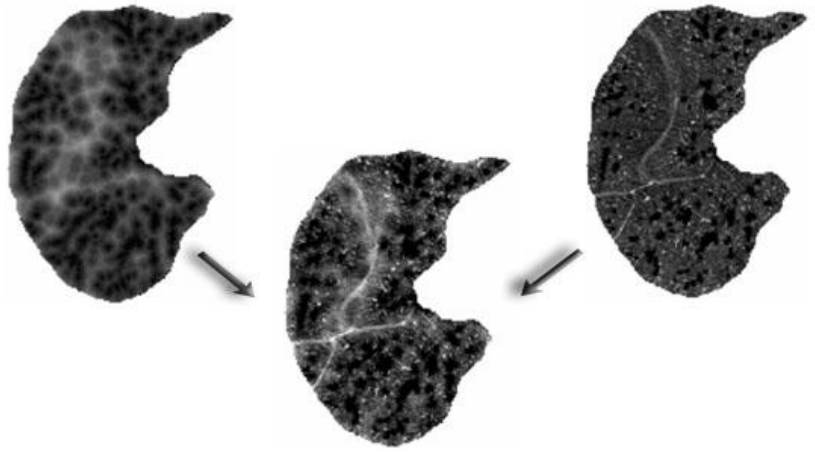

Figure 4. Combination of the 3D distance image D (left) and the original image I with the blood vessels masked out (right) to the new image C (center).

2.5. Interactive Watershed Transform

To finally obtain the lobar areas from the preprocessed image, a segmentation method is needed to allow the extraction of 3D-connected components separated by local maxima. Additionally, as mentioned in the introduction, the variety of representations and abnormalities with respect to the lobar anatomy can be expected to make user interaction necessary.

The multi-dimensional Interactive Watershed Transform (IWT) proposed by Hahn et al.[4] covers both aspects. The watershed algorithm's nature is to separate regions with intermediary areas of local maxima while the IWT in particular combines this feature with the necessary interactivity. It consists of two steps: First, all image elements are sorted according to their image intensity using a Bucket Sort algorithm. Second, each element is processed exactly once in the specified order with respect to its 6-neighborhood. The detected basins are hierarchically organized in a tree allowing efficient partitioning. Sorting, watershed transform, and tree generation are linear in time. After the watershed transform, an arbitrary number of markers is evaluated in real-time to control tree partitioning and basin merging.

To keep the interaction as small as possible, we want the information provided by those markers to be transported throughout the complete subtree belonging to the selected vessel. This is why we do not use the

image C directly as input for the IWT, but the image C' in which the vessels are inverted. $C' := (c'_v)_{v \in V}$ is formally defined by

$$c'_v := \begin{cases} M + c_v, & \text{ves}(v) = 0 \\ M - i_v, & \text{otherwise.} \end{cases} \tag{3}$$

where the value M denotes the maximum density value of any segmented vessel voxel. The effect of the inversion of the vasculature is that, due to the nature of the 3D watershed algorithm, the type of a marker placed on a large vessel close to the hilus will be spread along with the "rising water" through the lobar vessel subsystem. Thus, it gets distributed in all parts of the lobe before reaching the level M and successively flooding the parenchyma, eventually building the watersheds. It may still occur that one marker per lobe does not suffice to separate the vascular subsystems. But since the hierarchical data management of the IWT allows the results to be instantly updated and displayed, an incorrect segmentation can be noticed and corrected by the user immediately.

3. EXPERIMENTS AND RESULTS

So far, our method has been tested on CT scans of 24 different patients including many with pathologic findings such as tumors, emphysema, fibrosis and atelectasis. Hence the images originated from diverse clinics using different scanning facilities and protocols, their z-resolution was varying between 0.8 millimeters, using a multi-slice device, and 5 millimeters on conventional spiral CT scanners, whilst the x- and y-resolutions varied from 0.55 mm to 0.9 mm.

The proposed method was successfully applied to each of the 24 datasets. The number of markers necessary for the segmentation varied with the quality of the scan and the state of the patient's lungs. Placing one marker per lobe on a large vessel in close proximity to the hilus, we obtained results that, if not already satisfactory, could be corrected by merely adding a small number (usually 1 or 2) of extra markers.

We were not yet able to acquire manually generated segmentations for a comparison with the presented method. However, preliminary reproducibility studies have been conducted for one of the high resolution datasets (Siemens Volume Zoom, slice thickness 1.25 mm, voxel size $0.8 \times 0.8 \times 1.0$ mm^3) which, apart from an extra fissure and partially disintegrating fissures (see figure 5), showed relatively normal physiology.

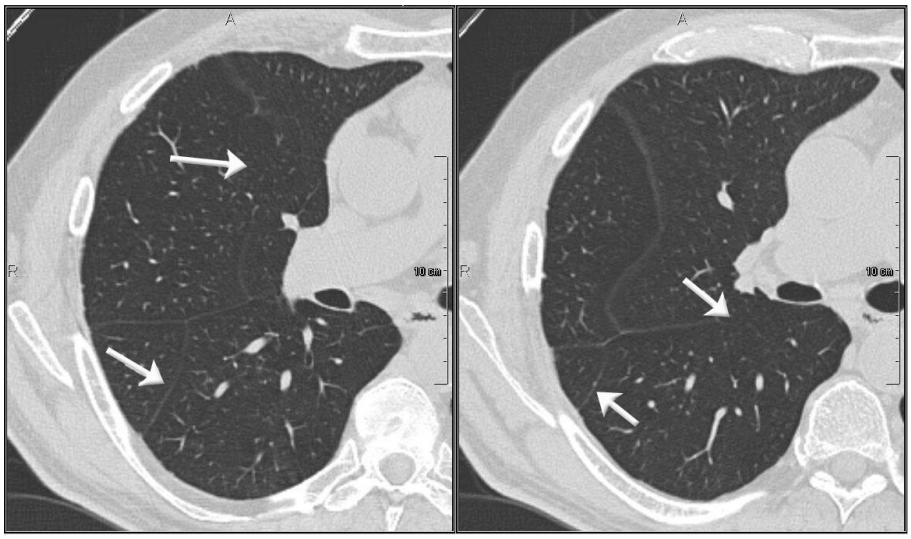

Figure 5. Sample slices of the processed dataset where two kinds of abnormalities are visible: disintegrating fissures (upper arrows) and an extra fissure (lower arrows).

First of all, an intra-observer study with $n = 5$ runs was performed on the right lung of the selected patient. No restriction on the number of markers was given, except that run 5 was specifically conducted using only one marker per lobe. The statistical analysis of the segmented lobe volumes displayed in table 1 shows a standard

deviation of below 0.5% per lobe. To more precisely verify the consistency of the segmentations, for each pair of results the similarity measure S was computed as follows: Let L be the number of voxels in the segmented lung, and let $\mathrm{cons}(R_1, R_2)$ denote the number of voxels within that lung which are classified consistently by the two segmentations R_1 and R_2, then we define the similarity $S(R_1, R_2)$ as the ratio of the consistent volume and the total lung volume:

$$S(R_1, R_2) = \frac{\mathrm{cons}(R_1, R_2)}{L}. \tag{4}$$

The similarity values are displayed in the upper right half of table 2, while the left lower half shows the lung volume classified consistently in each pair of runs in milliliters (using volumes instead of voxels will not alter the ratio, as long as the voxel size is constant throughout the volume).

Table 1. Volumetric results of the intra-observer study (right lung only). All values except those in the rightmost column are given in milliliters. μ denotes the average volume while σ refers to the standard deviation for the respective lobe.

Lobe	Run 1	Run 2	Run 3	Run 4	Run 5	μ	σ	σ (%)
lower	1785.03	1788.04	1784.54	1783.02	1787.68	1785.67	2.14	0.12
middle	654.92	653.96	655.42	655.44	648.06	653.56	3.13	0.48
upper	1351.53	1349.48	1351.52	1353.02	1355.73	1352.26	2.31	0.17

Table 2. Intra-observer study results. The total volume of the right lung obtained by the lung segmentation was 3791.48 ml. The left lower half of the table shows the volume (in ml) that was segmented consistently in two runs, while the upper right half displays the similarity value for each pair (i.e. the consistent volume divided by the total lung volume).

Runs	1	2	3	4	5
1	—	0.9979	0.9979	0.9988	0.9978
2	3783.63	—	0.9968	0.9975	0.9961
3	3783.53	3779.41	—	0.9974	0.9959
4	3786.97	3782.09	3781.72	—	0.9972
5	3783.32	3776.84	3775.99	3780.87	—

Additionally, an inter-observer study with $n = 5$ subjects was performed on the same data. There was again no restriction on the number of markers. The volumetric results displayed in Table 3 show a standard volume deviation of well below 1% per lobe. Again, the consistent volume and the similarity values were computed and displayed in Table 4.

Table 3. Volumetric results of the inter-observer study.

Lobe	User 1	User 2	User 3	User 4	User 5	μ	σ	σ (%)
lower	1789.40	1794.39	1786.06	1792.34	1786.96	1789.83	3.53	0.20
middle	652.50	645.68	655.39	646.60	651.07	650.25	4.07	0.63
upper	1349.58	1351.42	1350.03	1352.54	1353.45	1351.40	1.63	0.12

The algorithm was implemented and tested under Microsoft Windows 2000 on a Pentium IV with 1.7 GHz and 2 GByte of RAM. While the lung segmentation procedure takes about 3 minutes for the high resolution ($512 \times 512 \times 350$ voxels) chest dataset used in our studies, the lobe segmentation tool needed another 3 minutes to compute the input volumes for the watershed transform for both lungs*. The time spent for the following

*High resolution datasets were downsampled to speed up the computation.

Table 4. Inter-observer study results. The total volume of the right lung obtained by the lung segmentation was 3791.48 ml. The left lower half of the table shows the volume (in ml) that was segmented consistently by two users, while the upper right half displays the similarity value for each pair.

User	1	2	3	4	5
1	—	0.9977	0.9970	0.9956	0.9969
2	3782.79	—	0.9980	0.9974	0.9982
3	3780.20	3783.96	—	0.9974	0.9973
4	3774.65	3781.81	3781.49	—	0.9959
5	3779.79	3784.88	3781.08	3776.62	—

interactive lobe segmentation varied with the number of markers necessary for satisfactory results and ranged between 10 and 60 seconds per lung. Between the segmentation of both lungs, another 10 seconds are needed to save the results and to initialize the IWT with the combined image previously generated for the other lung.

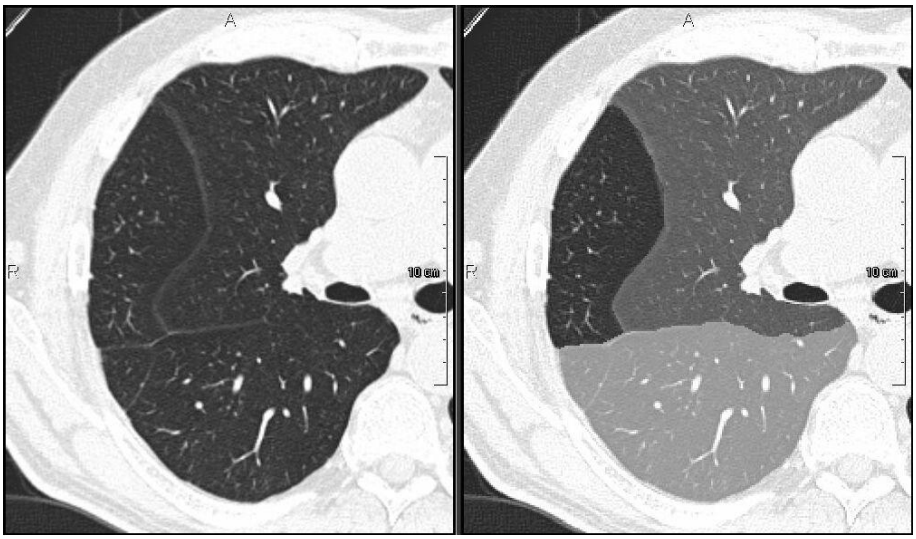

Figure 6. A single slice of the segmentation result (right image, results represented as overlays) for the right lung of the dataset processed in our studies, compared with the original slice (left). A 3D surface rendering of the results can be seen in Figure 1.

4. DISCUSSION AND FUTURE WORK

The preliminary intra- and inter-observer studies conducted already indicate a low variability (Similarity $>$ 99.5%) of the generated results. We are currently working on study protocols to further evaluate accuracy, reproducibility and usability of the proposed method. Additional studies to assess the prognostic value of lobe-based CT-parameters such as parenchyma volume or mean lung density for post-operative *Forced Expiratory Volume (FEV1)* in the case of lobar resection are planned.

To further improve the accuracy of our results, a more sophisticated vessel segmentation method would be helpful. An algorithm that is able to distinguish between vasculature and tumors or other structures with high density could further reduce the need for interaction (as long as the method itself is automated) and lead to more accurate results in difficult cases, which would most likely make up for the longer computational time to be expected. Moreover, in the case of processing high resolution datasets on a PC, the volume currently needs to be downsampled in order to make the memory demanding watershed transform run smoothly. This problem will

probably lose weight with the rapidly improving hardware, provided that the data resolution does not continue to increase at the same speed.

Due to the dependence of the proposed algorithm on the vascular structure, cases with vessels crossing from one lobe into another cause irregularities in the otherwise smooth boundaries. Although it is possible for the user to suppress these irregularities by introducing additional markers, such a procedure does not account for the physiological definition of lung lobes as being self-contained with respect to air and blood supply. Discussions with radiologists suggested that in fact the boundaries found by the algorithm without adjustment made more sense in a physiological way than the manually smoothed surfaces. Thus, the consideration of anatomic anomalies is a feature which cannot be provided by solely fissure- and atlas-based methods.

Concerning the amount of interaction necessary to obtain a satisfactory segmentation result, our method can certainly keep up with existing methods. Unlike most other semi-automated methods, the user interaction is carried out at the end of the procedure. This allows to instantly verify and, if necessary, correct the current result without any noticable recomputation delays. In conclusion, our approach introduces a robust lung lobe segmentation method that uses minimal and intuitive interaction. Decomposing the lungs into their lobar units not only assists in further image processing procedures such as lung segment detection or image registration, but also allows a more accurate prediction of functional parameters in case of a lobar resection, which is standard therapy for early stage lung cancer[†].

ACKNOWLEDGMENTS

We thank our clinical partners, Prof. Jend, Department of Diagnostic Radiology, Hospital Bremen-Ost, Prof. Thelen, Department of Diagnostic Radiology, University of Mainz, and Prof. Wein, Department of Diagnostic Radiology, University Hospital Aachen for providing us with high quality radiological data and giving the opportunity for many fruitful discussions. The research that lead to the presented results was conducted as part of the cooperation project VICORA – Virtual Institute for Computer Assisted Radiology (www.vicora.de).

REFERENCES

1. K. Hayashi, A. Aziz, K. Ashizawa, H. Hayashi, K. Nagaoki, and H. Otsuji, "Radiographic and CT appearances of the major fissures," *RadioGraphics* **21**, pp. 861–874, 2001.
2. L. Zhang and J. M. Reinhardt, "Detection of lung lobar fissures using fuzzy logic," in *Physiology and Function from Multidimensional Images*, C.-T. Chen and A. V. Clough, eds., *Proc. SPIE* **3660**, pp. 188–199, 1999.
3. L. Zhang, E. A. Hoffman, and J. M. Reinhardt, "Lung lobe segmentation by graph search with 3D shape constraints," in *Physiology and Function from Multidimensional Images*, C.-T. Chen and A. V. Clough, eds., *Proc. SPIE* **4321**, pp. 204–215, 2001.
4. H. K. Hahn and H.-O. Peitgen, "IWT – interactive watershed transform: A hierarchical method for efficient interactive and automated segmentation of multidimensional gray-scale images," *Proc. SPIE* **5032**(this volume), 2003.
5. S. Hu, E. A. Hoffman, and J. M. Reinhardt, "Automatic lung segmentation for accurate quantitation of volumetric x-ray ct images," *IEEE Transactions on Medical Imaging* **20**, pp. 490–498, June 2001.
6. D. Selle, *Analyse von Gefaessstrukturen in medizinischen Schichtdatensaetzen fuer die computergestuetzte Operationsplanung*, Shaker, Aachen, 1999.
7. T. Saito and J.-I. Toriwaki, "New algorithms for Euclidean distance transformation of an n-dimensional digitized picture with applications," *Pattern Recognition* **27**(11), pp. 1551–1565, 1994.

[†]except for Small Cell Lung Cancer (SCLC)